Thermodynamic Performance and Cost Optimization of a Novel Hybrid Thermal-Compressed Air Energy Storage System Design

Sammy Houssainy [1], Mohammad Janbozorgi [2], Pirouz Kavehpour [3]
[1] *National Renewable Energy Laboratory, 15013 Denver W Pkwy, Golden, CO 80401*
[2], [3] *Mechanical and Aerospace Engineering Department, University of California, Los Angeles, CA 46-147A Engineering IV, Los Angeles, CA 90095-1597, USA*

Abstract

Compressed Air Energy Storage (CAES) can potentially allow renewable energy sources to meet electricity demands as reliably as coal-fired power plants. However, conventional CAES systems rely on the combustion of natural gas, require large storage volumes, and operate at high pressures, which possess inherent problems such as high costs, strict geological locations, and the production of greenhouse gas emissions. A novel and patented hybrid thermal-compressed air energy storage (HT-CAES) design is presented which allows a portion of the available energy, from the grid or renewable sources, to operate a compressor and the remainder to be converted and stored in the form of heat, through joule heating in a sensible thermal storage medium. The HT-CAES design incudes a turbocharger unit that provides supplementary mass flow rate alongside the air storage. The hybrid design and the addition of a turbocharger have the beneficial effect of mitigating the shortcomings of conventional CAES systems and its derivatives by eliminating combustion emissions and reducing storage volumes, operating pressures, and costs. Storage efficiency and cost are the two key factors, which upon integration with renewable energies would allow the sources to operate as independent forms of sustainable energy. The potential of the HT-CAES design is illustrated through a thermodynamic optimization study, which outlines key variables that have a major impact on the performance and economics of the storage system. The optimization analysis quantifies the required distribution of energy between thermal and compressed air energy storage, for maximum efficiency, and for minimum cost. This study provides a roundtrip energy and exergy efficiency map of the storage system and illustrates a trade off that exists between its capital cost and performance.

1. Introduction

With the rising addition of renewable energy sources in the electrical grid, the integration of these sources has become increasingly challenging due to their intermittent nature. During surplus power generation, renewable sources are often curtailed for the safety and integrity of the electrical grid [1-6]. A logical solution would be to couple large-scale energy storage systems with renewable sources, which would reduce the curtailment and increase the capacity of wind turbines and photovoltaics. A large-scale energy storage system would allow the renewable sources to store excess power during periods of low demand, and provide the stored energy during periods of peak electricity demand. Therefore, allowing renewable sources to provide both base-load and peak-load markets. [7-11]

Among the numerous types of energy storage technologies, Compressed Air Energy Storage (CAES) and Pumped Hydro Storage (PHS) are most suitable for large-scale applications. However, CAES offers lower capital cost, lower maintenance cost, and fewer geological restrictions, rendering it more appealing as compared with PHS [12-15]. Much work has been devoted to analyzing various CAES derivatives, such as diabatic, isothermal, and advanced adiabatic CAES [16-21]. The categorization of these various CAES concepts is dictated by how heat is handled during compression and prior to expansion of the air. The only two exiting CAES plants in the world are based on the diabatic method, in which the heat of compression is not utilized in the system and is dissipated into the environment [22]. Therefore, diabatic CAES requires a heat source in the discharge process to prevent condensation and icing during expansion. The external heat source in diabatic CAES is provided by fossil fuels, therefore releasing greenhouse gas emissions. Consequently, diabatic CAES is a combined storage and generation system [23].

Isothermal CAES (I-CAES) aims to achieve true isothermal compression and expansion. I-CAES concepts are typically based on piston machinery, as they provide relatively longer times for more heat transfer. Heat exchange can be achieved through additional heat transfer surfaces and a liquid piston [24-27]. Open and closed cycle Hydro-Pneumatic Energy Storage (HyPES) systems are one type of I-CAES where liquid, such as hydraulic oil, performs the compression process. One major drawback of HyPES is its low energy density, which is the reason these systems have not been built commercially, however subject to laboratory-scale investigation [28-29]. Of the more attractive I-CAES proposals, one seeks to spray water droplets inside a reciprocating compressor to actively absorb

[1] Corresponding Author, Sammy.Houssainy@NREL.gov

the heat of compression [30]. However, such machinery has to be adjusted to endure water. Recent works investigate the compression of foam for better heat transfer [31].

In advanced adiabatic CAES (AA-CAES), the heat of compression is stored and reused during the discharge process. The absolute temperatures reached and stored, by the generated heat of compression in AA-CAES, have a major influence on the system design and performance. Moreover, the cycle efficiency is dependent on and increases with the absolute storage temperature [32-39]. Therefore, AA-CAES can be categorized into three types: 1) high temperature methods, with storage temperatures above 400C, 2) medium temperature methods, with storage temperatures between 200C to 400C, and 3) low temperature methods, with storage temperatures below 200C. A high temperature AA-CAES plant has two major challenges. First, increased engineering challenges arise when designing a TES unit that is capable of handling both high-temperature and high-pressure operations. Second, compressors capable of providing the exceedingly high temperatures are commercially unavailable [40-42]. In addition, the limited potential market demotivates research and development efforts of such machinery [43]. Medium and low temperature AA-CAES bypass the research and development efforts associated with high temperature compressors. In addition, the lower start-up times associated with such systems permit for involvement in additional auxiliary markets [44]. However, medium and low temperature AA-CAES concepts suffer from lower energy densities and lower roundtrip efficiencies [45-46].

Our novel and patented hybrid thermal and compressed air energy storage system is an extension of AA-CAES, where the heat of compression is stored and utilized during the discharge process. However, in HT-CAES the storage capacity is further increased by the direct conversion of electricity-to-heat in a high temperature TES unit, through joule/resistive heating. Because discharge temperatures of available off-the-shelf compressors are substantially lower than the maximum temperature of available TES mediums, these TES units cannot be fully utilized in AA-CAES [47]. In addition, compressors typically require a constant input power, corresponding to their design point, for optimal performance. Therefore, low quality, fluctuating, and highly intermittent renewable power signals that are inapplicable for compressors can be utilized through direct conversion to heat, which further increases the capacity of the HT-CAES system. In HT-CAES, part of the available energy is spent on operating the compressor(s), and the rest is directly converted to heat and stored in a High Temperature Thermal Energy Storage (HTES) medium. The HT-CAES configuration presented here also includes a turbocharger, on the discharge side, which provides supplementary mass flow rate alongside the air storage. Through our analysis we show that the addition of a turbocharger has the potential of drastically reducing the storage volume and pressure, which reduces the system complexity and cost, in addition to eliminating the need for multistage compression and expansion.

Compared with advanced adiabatic systems, the hybrid design has the following advantages: 1) Assuming identical machinery and air storage sizes, the hybrid design can provide higher output power through the additional stored heat, which would be neglected otherwise in an advanced adiabatic design, 2) The necessary storage volume/pressure can be reduced due to the increased capacity of the system and by the addition of the turbocharger, which reduces the geological restrictions of the plant, 3) the complexity is reduced by mitigating the need for high temperature compressor research and development, and by alleviating the need for multi-stage compression and expansion, 4) it will be shown that with increased dependence on thermal storage the system cost is substantially reduced.

In generally, the cost of thermal storage is substantially lower than the cost of air storage, per kilowatt-hour [48]. However, a heat engine is theoretically lower in efficiency than a CAES plant. Therefore, with increased reliance on thermal storage, through the turbocharger, the HT-CAES system cost and efficiency are anticipated to decrease. The goal of this work is to provide an efficiency and cost map of the HT-CAES system versus both the operating pressure and the distribution of energy, between thermal and compressed air storage. This work will illustrate and properly quantify a tradeoff that exists between the HT-CAES system cost and performance. Both roundtrip energy and exergy efficiencies are quantified, presented, and compared. Lastly, a local optimum-line of operation, which results in a local maximum in efficiency and a local minimum in cost, is presented.

2. Methods

Figure 1 represents the HT-CAES thermodynamic cycle that is analyzed here. During the charge process electricity from renewable sources, or the gird, is used to operate the compressor. Simultaneously or subsequently, depending on available power during the charge process, electricity is converted directly into thermal energy, through joule/resistive heating, and is stored in the High Temperature Thermal Energy Storage (HTES) unit. The HTES unit

takes advantage of the high thermal capacity of an inexpensive thermal medium to store heat that will later be used to heat up the compressed air out of the air storage. Conversion of electricity to thermal energy can result in very high temperatures and thus high energy densities when the energy is well contained. As a result, temperatures and volumetric energy densities well in excess of traditional CAES and AA-CAES can be achieved, while the size of the air storage can be reduced. The practical limit on how high a temperature can be reached in the HTES is defined by the material properties of the storage and the electric wires. Alumina-based refractory provides service temperatures in excess of 1700C and Nichrome wires can have a continuously operating temperature of ~ 1680C. With the addition of an HTES unit, the workload is shifted from pure compression to investing partially in thermal storage. This separation of energy storage between compressed air and thermal storage has the effect of expanding the energy capacity of the compressed air system without the need to increase the air pressure or air storage capacity. The HTES also allows the system to be dynamically scaled up or down as the load leveling demand changes without any structural change in system configuration.

In addition to the direct electricity-to-heat conversion and storage, accomplished by the HTES, the heat of compression is also stored separately in a Low Temperature Thermal Energy Storage (LTES), which is essentially a two-tank system. Initially during the charge process, tank "a" is filled with a cold Heat Transfer Fluid (HTF) and tank "b" is empty, shown in Figure 1. As the air is being compressed, tank "a" is discharged and the HTF collects the heat of compression via the LTES charge heat exchanger. The hot HTF is then stored in tank "b" for later use during the discharge process. During the discharge process, air is released from the cavern/tank and subsequently maintained at a constant process pressure, via Joule-Thomson throttling, through the pressure-regulating valve. The process pressure is herein referred to as the prime pressure. The temperature of the discharging air is then raised through three successive stages of heating before entering the expander: LTES, regenerator, and HTES. Additionally during the discharge process, a turbocharger is utilized which provides supplementary mass flow rate alongside the air storage. This has multiple advantages: 1) the storage system does not purely rely on the mass flow rate provided by the cavern 2) the necessary storage volume can be significantly reduced, which alleviates the restriction on geological locations 3) storage pressures can be drastically reduced, which has profound impacts on the lifetime, reliability and practicality of implementation 4) the cost of the system can be considerably reduced, as the system cost becomes leveraged by the price of thermal storage, which is typically cheaper than CAES [49].

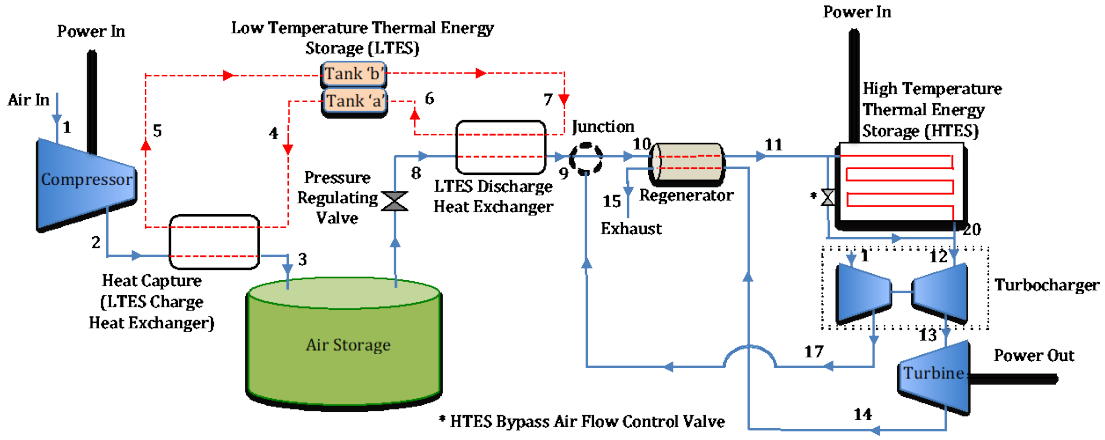

Figure 1: Patented Hybrid Thermal and Compressed Air Energy Storage Process Diagram [50]

Throughout this paper, the prime pressure, P_{prime}, is defined as the minimum air storage pressure and the discharge operating/process pressure, adjusted by the pressure-regulating valve. Hence, the prime pressure delineates the expansion and compression ratios of the turbine and turbocharger compressor, which dictates their exhaust temperatures T_{14}, T_{17} shown in Figure 1. Therefore, the placement order of the regenerator, LTES discharge heat exchanger, and turbocharger junction on the discharge side of Figure 1 is one possible configuration. In this analysis however, depending on the chosen prime pressure, the configuration order of the LTES discharge heat exchanger, regenerator, and junction, is rearranged such that successive heating is always attained.

2.1 Problem Statement

As described, the novel hybrid storage system presented here allows a portion of the available energy, from the grid

or renewable sources, to operate a compressor and the remainder to be converted and stored directly in the form of heat by the HTES. The premise of this paper is to optimize this distribution of energy between compressed air energy storage and thermal energy storage for maximum efficiency, and for minimum cost. To properly quantify the distribution of energy between thermal and compressed air energy storage we define the variable β, which represents the fraction of energy converted and stored in the form of heat through the HTES, Q_{HTES}, over the total amount of energy stored in the system; the energy of compression, W_{Comp}, plus electricity-to-heat conversion and storage, Q_{HTES}.

$$\beta = \frac{Q_{HTES}}{W_{Comp} + Q_{HTES}} \tag{1}$$

The optimization analysis is achieved through a parametric study of the energy allocation fraction, defined by β, and examining its effects on the performance, cost, component sizing, and various other parameters that characterize the hybrid storage system. In addition to β, the prime pressure is also investigated as its variation leads to important and conclusive design guidelines.

2.2 Assumptions

Pressure losses within the pipes were not taken into account and all components, besides the air storage and HTES, are assumed to operate quasi-steadily during charge and discharge. The rational is that the residence time within these components is much shorter than charge and discharge time scales, indicated in Table 1. Also, heat capacities are assumed to be temperature independent and isentropic component efficiencies are incorporated. Table 1 summarizes the additional constants used throughout the investigation presented here.

Table 1: Thermodynamic Constants

Property	Value	Units	Description
P_1	1	Bar	Atmospheric Pressure
T_1	300	K	Atmospheric Temperature
P_2	20	Bar	Maximum Air Storage Pressure
T_4	300	K	LTES Inlet HX Temperature During Charge
T_{12}	1000	K	Turbocharger Inlet Temperature
T_{min}	1000	K	HTES Primed/Initial/Minimum Temperature
T_{max}	1600	K	HTES Maximum Temperature (End of Charge)
t_{charge}	6	Hours	Charge Time
$t_{discharge}$	6	Hours	Discharge Time
W_{output}	100	MW	Power Output Provided by the System
$\varepsilon_{d,LTES}$	0.8	-	LTES Discharge Heat Exchanger Effectiveness
$\varepsilon_{c,LTES}$	0.8	-	LTES Charge Heat Exchanger Effectiveness
η_c	0.75	-	Compressor Isentropic Efficiency
η_{Dcomp}	0.75	-	Turbocharger Compressor Isentropic Efficiency
η_t	0.8	-	Turbine Isentropic Efficiency
η_r	0.8	-	Regenerator Effectiveness
c_{HTES}	0.88	kJ/kg K	Specific Heat Capacity of HTES
R	0.287	kJ/kg K	Specific Gas Constant of Air
c_v	0.718	kJ/kg K	Specific Heat Capacity of Air at Constant Volume
c_p	1	kJ/kg K	Specific Heat Capacity of Air at Constant Pressure

It is imperative to note that the maximum air storage pressure, P_2=20bar, assumed in this analysis is considerably lower than that of conventional (~70bar) and advanced adiabatic (>70bar) compressed air energy storage systems. A detailed outline of the calculations made for each component in the cycle is presented next; this includes all significant equations and any component specific assumptions.

3. Calculations

The general mass and energy balance equations together with the calorically perfect gas equations of state are given below:

$$\frac{dM}{dt} = \dot{m}_{in} - \dot{m}_{out} \tag{2}$$

$$\frac{dE}{dt} = \dot{m}_{in}h_{in} - \dot{m}_{out}h_{out} + \dot{Q} - \dot{W} \tag{3}$$

$$PV = MRT \tag{4}$$

Where

$$E = Me \tag{5}$$
$$e = c_v T \tag{6}$$
$$h = c_p T \tag{7}$$

Where e and h are the specific energy and enthalpy, and M is the mass of air. The isentropic relation, for an ideal and calorically perfect gas, relating pressure and temperature is below

$$\frac{T_2}{T_1} = \left(\frac{P_2}{P_1}\right)^{\frac{k-1}{k}} \tag{8}$$

3.1 Compressor

A constant compression ratio and flow rate is assumed in the compressor model. Additionally, adiabatic conditions are assumed, which result in a constant compression power with a mass flow rate given by equation (9). The compression mass flow rate, given by equation (9), is obtained by utilizing an energy balance, equation (3), and the calorically perfect and ideal gas relation given by equations (7) and (8).

$$\dot{m}_{charge} = \frac{\eta_c}{c_p T_1 \left(\left(\frac{P_2}{P_1}\right)^{\frac{k-1}{k}} - 1\right) t_{charge}} W_{comp} \tag{9}$$

Where η_c is the isentropic compressor efficiency, k is the ratio of specific heats for air, P_2 and P_1 are the maximum air storage and ambient pressures respectively, T_1 is the ambient temperature, c_p is the specific heat of air at constant pressure, and t_{charge} is the charge time. Lastly, W_{comp} is the total allocated compression energy, which is a function of β; therefore, the charge mass flow rate, given by equation (9), is also a function of β. The coefficient of W_{comp} in equation (9) is a constant, the value of which can be obtained through the constants in Table 1. The compressor exhaust temperature is obtained by utilizing the isentropic compressor efficiency, defined as the ratio of isentropic work over actual work, the isentropic relation given by equation (8), and the calorically perfect gas equation (7), resulting in equation (10)

$$T_2 = \frac{T_1\left(\left(\frac{P_2}{P_1}\right)^{\frac{k-1}{k}} - 1\right)}{\eta_c} + T_1 \tag{10}$$

3.2 LTES

The Low Temperature Thermal Energy Storage (LTES), as explained previously, is a two-tank system containing and circulating a Heat Transfer Fluid (HTF), which collects the heat of compression during charge, and withdraws the heat during the discharge process. Tank 'a' is assumed in thermal equilibrium with the environment and tank 'b' is assumed adiabatic, shown in Figure 1. Utilizing the constant heat exchanger effectiveness, $\varepsilon_{c,LTES}$, provided by Table 1, and an energy balance, through equation (3) and (7), the inlet and exit LTES heat exchanger temperature streams, corresponding to points 3 and 5 in Figure 1, can be obtained and are given by equations (11) and (12)

$$T_3 = T_2 - \varepsilon_{c,LTES}(T_2 - T_4) \tag{11}$$
$$T_5 = \frac{\dot{m}_{charge} c_p}{\dot{m}_{c,LTES} c_{LTES}}(T_2 - T_3) + T_4 \tag{12}$$

Where $\dot{m}_{c,LTES}$ is the LTES charge mass flow rate and c_{LTES} is the specific heat of the HTF. All subscripts correspond to the process diagram in Figure 1. The heat capacity rate of the air and LTES HTF are assumed equal. Moreover, tank 'b' is assumed adiabatic, therefore T_5=T_7 in Figure 1. The temperatures in the vicinity of the LTES discharge heat exchanger and the regeneration component are calculated similarly, by applying an energy balance, assuming adiabatic conditions, and considering the heat exchanger effectiveness provided in Table. 1.

3.3 Air Storage

The air storage volume is calculated through an energy balance assuming an adiabatic, ideal, and calorically perfect

gas. Utilizing equations (3)-(6) it can be shown that during the charge process the necessary air storage volume, which operates at a specified pressure swing, $\Delta P = P_2 - P_{prime}$, is

$$V_{Air\ Storage} = \frac{kRT_3 t_{charge}}{P_2 - P_{prime}} \dot{m}_{charge} \tag{13}$$

Where P_{prime} is the minimum storage pressure and P_2 is the maximum storage pressure, given in Table 1. The calculated results given by equations (9) and (11) are used to determine the air storage volume in equation (13). The mass flow rate, given by equation (9), is a function of the energy fraction, β, therefore the air storage volume, specified by equation (13), is also a function of β. The air storage discharge mass flow rate is determined through an energy balance assuming an adiabatic, ideal, and calorically perfect gas. Utilizing equation (3)-(6), where M_o is the initial stored air mass determined through the ideal gas equation (4), it can be shown that

$$\dot{m}_{discharge} = \frac{M_o + t_{charge}\dot{m}_{charge}}{t_{discharge}} \left[1 - \left(\frac{P_{prime}}{P_2}\right)^{\frac{1}{k}}\right] \tag{14}$$

The air storage is initially assumed at a specified prime pressure, P_{prime}, and ambient temperature. The air storage is inherently transient therefore the time dependent temperatures and pressures must be calculated as the discharging air passes through the various downstream components. Through the mass and energy balance, equations (2) and (3), together with the calorically perfect gas equations of state, given by equations (4)-(7), the following discretized equations are used to determine the time dependent temperature and pressure of the discharging air

$$u(t + \Delta t) = \frac{M(t)u(t)}{M(t + \Delta t)} + \frac{M(t + \Delta t) - M(t)}{M(t + \Delta t)} h(t) \tag{15}$$

$$T(t + \Delta t) = \frac{u(t + \Delta t)}{c_v} \tag{16}$$

$$P(t + \Delta t) = \rho(t + \Delta t) \cdot R \cdot T(t + \Delta t) \tag{17}$$

The initial temperature of the discharging air is found by incorporating the ideal gas law given the specified maximum pressure in Table 1, the calculated volume from equation (13), and the total stored mass. The air storage is discharged until the specified prime pressure, P_{prime}, is reached.

3.4 Turbocharger

The purpose of the turbocharger is to provide supplementary mass flow rate, at the junction in Figure 1, in addition to the discharging cavern/tank flow rate. The total discharge flow rate, which enters the HTES and turbine, is therefore the sum of both discharging cavern/tank mass flow rate plus supplementary mass flow rate provided by the turbocharger. Through an energy and mass balance, on a control volume containing the turbocharger and power turbine, the total necessary discharge mass flow rate is obtained and is given by equation (18)

$$\dot{m}_t = \frac{\dot{W}_{output} - \dot{m}_{discharge} c_p (T_{17} - T_1)}{c_p (T_{12} - T_{14}) - c_p (T_{17} - T_1)} \tag{18}$$

Where $\dot{W}_{output}$, T_{12}, T_1 and c_p are constants specified by Table 1, and $\dot{m}_{discharge}$ is given by equation (14). The compressor and turbine exhaust temperatures, T_{14} and T_{17}, are obtained by employing the isentropic compressor and turbine efficiencies given in Table 1, similar to the procedure which arrived at equation (10).

3.5 HTES

The high temperature thermal energy storage (HTES) is inherently a transient component. However, the HTES can be designed to deliver a constant temperature, necessary for optimal operation of a turbo-expander, through bypassing a portion of the cold inlet air with the hot flow exiting the HTES, as shown in Figure 1. Applying the energy and mass balance to the point where the bypass line mixes with the hot flow out of the HTES, the bypass mass flow rate, $\dot{m}_{bp}(\mathrm{t})$, can be obtained as a function of $T_{20}(t)$ and T_{12}:

$$\dot{m}_{bp}(t) = \dot{m}_t \frac{T_{20}(t) - T_{12}}{T_{20}(t) - T_{11}(t)} \tag{19}$$

Where $T_{20}(t)$ is the time dependent temperature of the HTES. For simplicity, and as a first order approximation, a lumped capacitance approximation is used to model the HTES, where no temperature gradients exist within the HTES. Additionally, it is assumed that at each instant of time during the discharge process the exit air temperature is equal to the instantaneous HTES temperature. The amount of energy allocated to the HTES, $Q_{\beta,HTES}$, is used to size its mass such that its maximum specified temperature is reached at the end of charge as follows

$$M_{HTES} = \frac{Q_{\beta,HTES}}{c_{HTES}(T_{max} - T_{min})} \tag{20}$$

The total energy that must be stored by the hybrid storage system, to deliver the constant energy output specified in Table 1, must be iteratively solved at each specified β. This is because the sought-after efficiency of the system is inherently a function of β as made clear by equation (21)

$$E_{input}(\beta) = \frac{E_{output}}{\eta_I(\beta)} \tag{21}$$

The first law efficiency, or equivalently the roundtrip energy efficiency, η_I, is defined as the total output energy over the total input energy, thermal plus compression. E_{input} and E_{output} are the total input and output energies. The bisection method is used to iteratively solve for the necessary input energy, such that the final HTES temperature, at the end of discharge, reaches precisely the minimum value specified in Table 1.

3.6 Roundtrip Energy and Exergy Efficiencies

The roundtrip energy efficiency (1st law efficiency) of the system is defined on an energy basis as the total output over total input energy as shown by equation (22).

$$\eta_I = \frac{\int \dot{W}_{output}\, dt}{\int \dot{W}_{comp} dt + \int \dot{Q}_{HTES}\, dt} \tag{22}$$

Similarly, the roundtrip exergy efficiency (2nd law efficiency) is defined as the total output over total input exergy, as shown by equation (23).

$$\eta_{II} = \frac{\int \dot{W}_{output}\, dt}{\int \dot{W}_{comp} dt + \int (1 - T_o/T_{HTES}) \dot{Q}_{HTES}\, dt} \tag{23}$$

The exergy associated with compression and expansion is equivalent to their energy values, assuming adiabatic conditions. However, the exergy associated with heat transfer in the HTES is determined by the second term in the denominator of equation (23). For simplicity, assuming no temperature gradients within the HTES and a constant input electrical signal, the exergy associated with heat transfer can be calculated by first determining the HTES temperature, T_{HTES}, during the charge process using the energy balance equation (3). Performing the Integration in equation (23) and utilizing the 1st law efficiency and β definitions, through equation (22) and (1), results in equation (24)

$$\eta_{II} = \frac{\eta_I}{1 - T_o \beta \ln(1 + \delta/T_{\min})/\delta} \tag{24}$$

Where T_o is the ambient temperature, $T_{\min}$ is the minimum HTES temperature, and δ is the maximum HTES temperature difference, $\delta = T_{\max} - T_{\min}$. The 2nd law efficiency of the system, equation (24), is presented conveniently as a function of the 1st law efficiency, η_I, the energy distribution fraction, β, and the HTES periphery temperatures. By observing the 2nd law efficiency, equation (24), it becomes immediately apparent that all variables in the denominator are positive. Therefore, the 2nd law efficiency is always greater than or equal to the 1st law

efficiency, $\eta_{II} \geq \eta_I$, which is consistent with the exergy efficiency of heat engines.

3.7 Cost Functions

The following cost functions, based on thermodynamic variables, are used to determine the purchase price of the compressors and turbines [51], [52].

$$\Xi_{\text{compressor}} = \text{c}_1 \frac{39.5\,\dot{m}}{0.9 - \eta_c} r_c \ln(r_c) \tag{25}$$

$$\Xi_{\text{turbine}} = \text{c}_1 \frac{266.3\,\dot{m}}{0.92 - \eta_t} \ln(r_e)(1 + \exp(0.036 T_{\text{inlet}} - 54.4 c_2)) \tag{26}$$

Where r_c and r_e are the compression and expansion pressure ratios and the constants, c_1=1.051 c_2=1.207, reflect costs reported by the Gas Turbine World Handbook [51], [52]. The cost of air storage through an above ground tank typically scales with volume and pressure, however, with a fixed maximum pressure throughout this study, the cost function for a tank as a function of volume, based on multiple vendors (Fjords Processing, KS Industries, Modern Custom Fabrication Inc.), is below

$$\Xi_{\text{Air Storage}} = 1000\, V_{tank} \tag{27}$$

The cavern cost function, based on volume, is shown below [23]

$$\Xi_{\text{Air Storage}} = 3.75 \times 10^7 + 62\, V_{cavern} \tag{28}$$

In this analysis the cheapest air storage architecture, based on the above cost functions, is utilized. Lastly, the HTES is an alumina-based refractory with a material purchase cost, based on mass and determined through various vendors (Resco Products, Harbison-Walker Refractories), given by the cost function below

$$\Xi_{\text{HTES}} = 2.2 M_{HTES} \tag{29}$$

In addition to the above cost functions, a factor of 1.25 is multiplied to account for the remaining heat exchangers, pipes, valves, LTES HTF and tanks. The total system capital cost per kilowatt-hour is given below

$$Cost\left[\frac{\$}{kWh}\right] = \frac{(\Xi_{\text{compressor}-1} + \Xi_{\text{compressor}-2} + \Xi_{\text{turbine}-1} + \Xi_{\text{turbine}-2} + \Xi_{\text{Air Storage}} + \Xi_{\text{HTES}}) \times 1.25}{E_{output}} \tag{30}$$

Where two compressor and turbine cost functions are considered, as evident by Figure 1. The denominator represents the total delivered energy, obtained by multiplying the total discharge time by the constant output power, as specified in Table 1.

4. Results

As stated in the Problem Statement section 2.1, the premise of this study is to investigate the performance and cost of the hybrid energy storage system as the energy distribution between thermal and compressed air energy storage is varied. The distribution of energy is quantified through the variable β, equation (1). The extreme case of β=100% results in pure thermal energy storage, as no energy is allocated towards compression, and the air storage does not receive or provide any air mass flow. Therefore, in the case where β=100% the process diagram, in Figure 1, becomes a regenerative Brayton cycle. Conversely, the case of β=0% results in pure compressed air energy storage, with no energy allocated to the HTES. In addition to analyzing the ramifications of β on the performance and cost of the system, the prime pressure is also investigated. The prime pressure, P_{prime}, represents the minimum air storage pressure and the discharge operating pressure, which is adjusted through the pressure-regulating valve, as shown in Figure 1. The two variables under investigation β and P_{prime} are of particular interest as their variation lead to noteworthy and definitive design guidelines.

4.1 Roundtrip Energy and Exergy Efficiencies

The roundtrip energy efficiency (1st law efficiency) map of the HT-CAES system, and its corresponding contour plot, is provided in Figure 2. As stated previously, in the extreme limit of β=100%, where the energy is stored purely in the form of heat through the HTES, the hybrid storage system becomes a regenerative Brayton cycle. Moreover,

in a regenerative Brayton cycle, with a constant power output and turbine inlet temperature, there exists an optimum operating pressure (prime pressure, P_{prime}) leading to maximum energy efficiency. This is equivalent to, and validates, the profile in Figure 2 at β=100%.

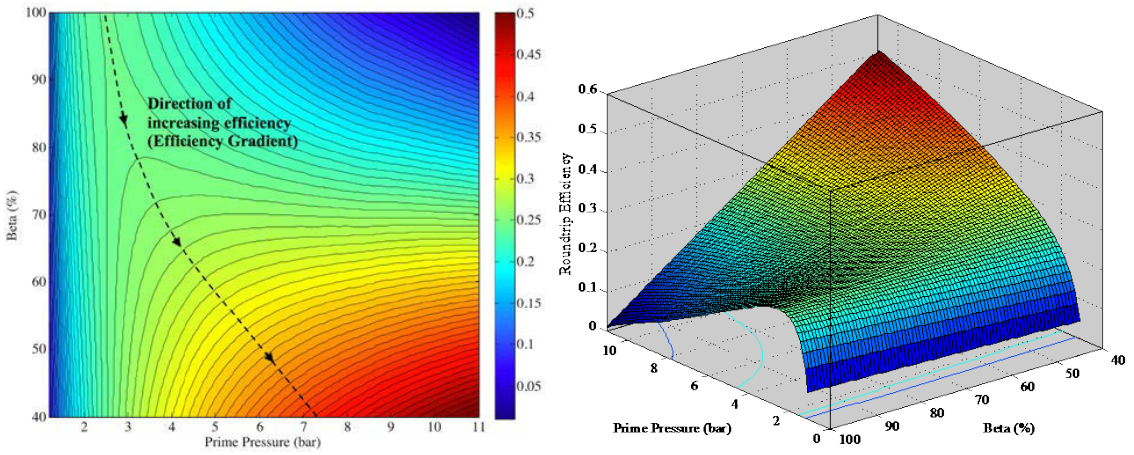

Figure 2: HT-CAES roundtrip energy efficiency map as a function of the energy distribution fraction, β, and the prime pressure, P_{prime}. The dotted line represents the direction of increasing efficiency (efficiency gradient, $\nabla\eta(\beta, P_{prime})$), which begins at the optimum design point of a regenerative Brayton cycle (at $\beta = 100\%$).

As the operating pressure increases, at β=100%, eventually regeneration becomes ineffective as the turbine exhaust temperature falls below the turbocharger compressor exhaust temperature. At which point regeneration is disengaged and a classical Brayton cycle is employed at higher operating pressures, resulting in slightly higher efficiencies, nevertheless, eventually leading to zero efficiency. A Brayton cycle at a constant turbine inlet temperature of 1000K, power output of 100MW, and isentropic efficiencies corresponding to the constants in Table 1, reaches an efficiency of zero at an operating pressure of 11.3bar and is not operational for higher operating pressures. In general, the efficiency of the hybrid storage system increases with decreasing β; as the reliance on compressed air storage increases. This is because a hybrid CAES system is theoretically more efficient than its corresponding Brayton cycle counterpart. Additionally, CAES systems are generally not bound by the Carnot efficiency, as is the case for heat engines. Furthermore, as β increases, a larger fraction of the discharge flow rate is provided by the turbocharger, which introduces additional isentropic component efficiencies that impede the roundtrip energy efficiency of the system. The efficiency of the hybrid storage system increases with the operating pressure at the lower end of the β spectrum, corresponding to higher compressed air storage dependence, as illustrated in Figure 2. The reason behind the monotonic increase in efficiency with operating pressure, at lower β values, stems from the accompanying decrease in throttling losses and exhaust temperatures.

At β values below 40%, the amount of energy allocated towards the HTES becomes too low for proper operation. This is because the HTES mass, which is calculated based on the specified temperature swing in Table 1, decreases with decreasing β; as the energy allocated for thermal storage decreases. Eventually, the HTES mass becomes too low and drops below the minimum specified temperature at the end of discharge, and therefore cannot bear the total discharging flow rate. Hence, β values below 40% are not investigated. Beginning with the optimum prime pressure of a regenerative Brayton cycle, at β=100% in Figure 2, and moving along the direction of increasing efficiency or efficiency gradient, results in the dotted line shown in Figure 2. Any perpendicular deviation along this efficiency gradient results in a lower efficiency than otherwise achievable. The significance of this efficiency gradient curve will be demonstrated and revisited when discussing the capital cost of the system, in section 4.3.

The roundtrip exergy efficiency (2nd law efficiency) contour map of the HT-CAES system is provided in Figure 3.

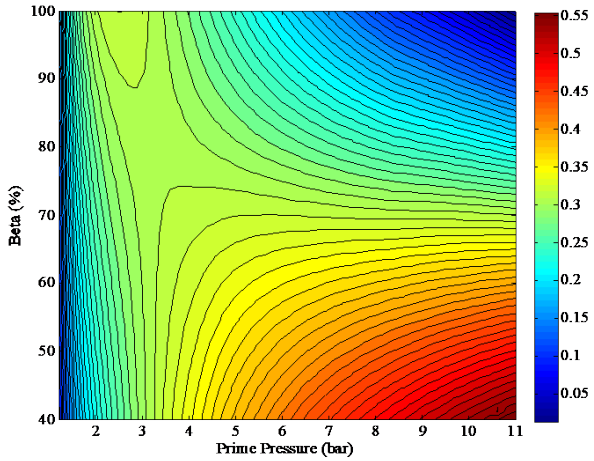

Figure 3: HT-CAES roundtrip exergy efficiency contour map as a function of the energy distribution fraction, β, and the prime pressure.

The HT-CAES exergy efficiency is always greater than its energy efficiency, a result that is consistent with heat engines. The energy and exergy efficiencies become coincident in the limiting case of a very large HTES temperature swing, $\delta = T_{max} - T_{min}$, as indicated by equation (31).

$$\lim_{\delta \to \infty} \eta_{II} = \eta_I \tag{31}$$

Therefore, the minimum exergy efficiency is equal to its corresponding energy efficiency, $\eta_{II,min} = \eta_I$. This is due to the increase in internal irreversibilities associated with mixing losses in the HTES at a high temperature swing; a result that is undetected through the first law analysis and efficiency. Conversely, the largest difference in 1st and 2nd law efficiencies (in other words, the maximum exergy efficiency for a given energy efficiency) occurs in the limit of a very low HTES temperature difference, meaning the HTES remains isothermal, and internal irreversibilities associated with mixing losses are eliminated, as shown by equation (32)

$$\lim_{\delta \to 0} \eta_{II} = \frac{\eta_I}{1 - \beta \frac{T_o}{T_{HTES}}} \tag{32}$$

Further increase in their difference occurs for 1) high β values, and 2) at lower HTES temperatures. Since the exergy efficiency is defined as a comparison of the system performance to the ideal case, at high β values the system is utilizing a lower quality of energy (heat), therefore for the same energy efficiency the result is higher exergy efficiencies. In the limit that $\delta = T_{max} - T_{min} = 0$, by definition this means the HTES remains isothermal, $T_{min} = T_{max} = T_{HTES}$. As a mathematical consequence, with a lower HTES temperature the second term in the denominator of equation (23) is at a minimum, which leads to maximum exergy efficiency for a given energy efficiency. However, the physical meaning can be explained as follows: at a low HTES temperature the system is utilizing a lower quality of heat, therefore for the same energy efficiency the result is higher exergy efficiencies.

4.2 Component Sizing

The various mass flow rates of the system, the air storage volume, and the thermal storage mass are presented in this section. The charge and discharge mass flow rates into and out of the cavern/tank are plotted, in Figure 4, as functions of the prime pressure and the energy distribution fraction. The charging mass flow rate, into the air storage, is identically zero at β=100% as no energy is allocated and stored in the form of compression, Figure 4. In general, the charge mass flow rate increases with decreasing β as more energy is allocated towards compressing and storing air. In addition, at higher roundtrip efficiencies the amount of output power per kilogram of air is also higher; meaning, for a constant power output the necessary mass flow rate is lower. Consequently, at the lower end of the β spectrum, the charge mass flow rate decreases with prime pressure, as a result of the increase in efficiency, as evident by Figure 2 and 3. The discharging mass flow rate provided by the air storage is nearly identical to the charge mass flow rate, as the air storage is assumed adiabatic. Therefore, the trends of the discharging mass flow

rate, as a function of β and the prime pressure, are the same as those described previously for the charging flow rate. The analysis performed here is of the first cycle, however after several cycles the air storage no longer experience cyclic variations, at which point the charge and discharge mass flow rates become identical.

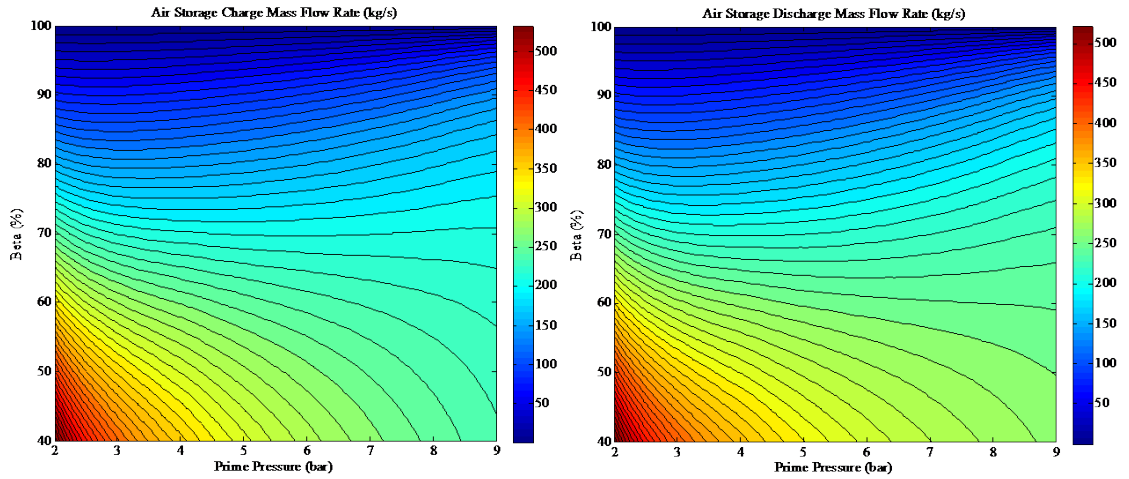

Figure 4: HT-CAES air storage, charge and discharge, mass flow rates as a function of the energy distribution, β, and the prime pressure

The turbine and turbocharger mass flow rates are plotted in Figure 5 as functions of the energy distribution fraction and the prime pressure. As depicted by Figure 5, the turbine mass flow rate generally decreases with decreasing β. Moreover, the turbine mass flow rate, at the higher β spectrum, reaches a minimum value as a function of the prime pressure and decreases with increasing prime pressure at the lower β spectrum. The turbine mass flow rate resembles the opposite trend depicted by the roundtrip efficiency. This is because the total and necessary mass flow rate through the turbine is largely influenced by the roundtrip efficiency of the system. The total mass flow rate is inversely proportional to the roundtrip storage efficiency, since the total power output per kilogram of air is higher at regions of higher efficiency, which for a constant power output results in lower mass flow rates. Conversely, the total power output per kilogram is lower at regions of lower efficiency, which for a constant power output results in higher necessary mass flow rates.

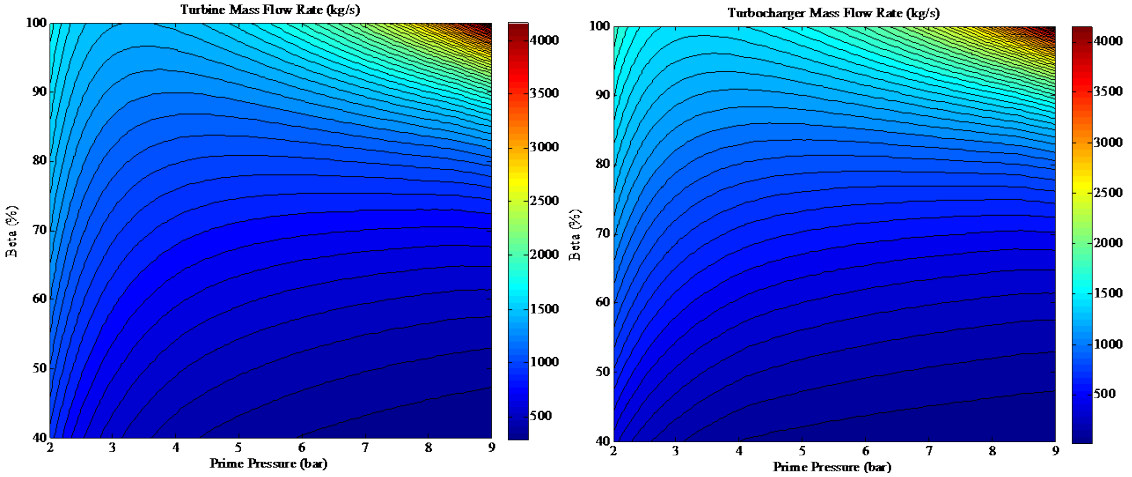

Figure 5: HT-CAES turbine and turbocharger, mass flow rates as a function of the energy distribution, β, and the prime pressure

The necessary turbocharger mass flow rate, in general, decreases with decreasing β values. By definition, as β decreases the reliance of the flow rate on the turbocharger decreases as the air storage provides a larger fraction of the total flow rate. The turbocharger mass flow rate map is largely influenced by the total turbine mass flow rate, as it is defined as the difference between the total and the stored air discharge mass flow rate.

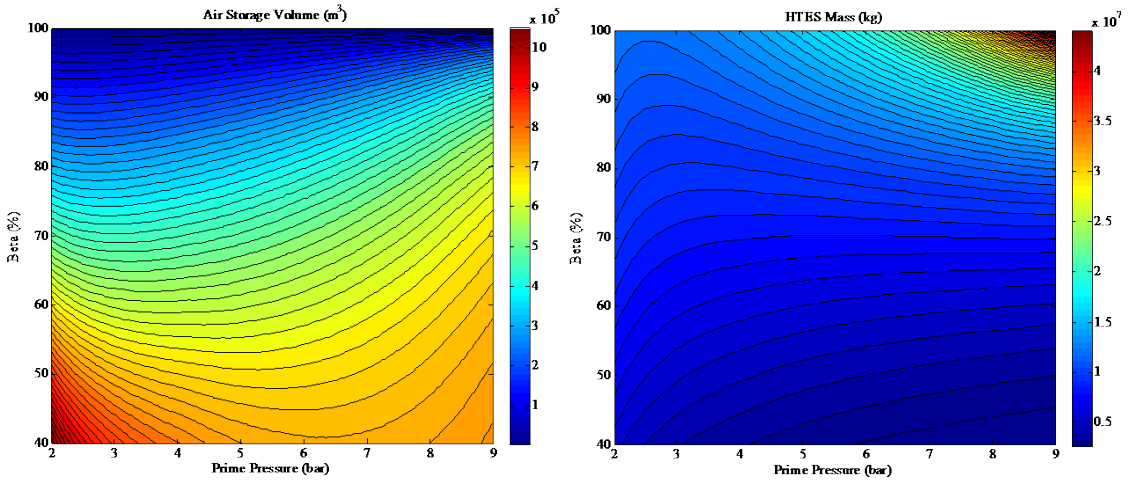

Figure 6: HT-CAES air storage volume and thermal storage mass as a function of the energy distribution, β, and the prime pressure

The air storage volume, Figure 6, generally increases with decreasing β; this is because the reliance on the compression energy increases with decreasing β. At β=100%, the air storage volume is identically zero, as the system evolves into a regenerative Brayton cycle. As β values decrease from 100%, the volume increases with the prime pressure and the total compression energy, as depicted by equation (13). The compression energy, for a fixed β value, is inversely proportional to the roundtrip efficiency of the system. Therefore, the air storage volume, at constant β, is proportional to the prime pressure and inversely proportional to the roundtrip efficiency of the system. The competition between the efficiency of the system and its prime pressure leads to a minimum air storage volume illustrated in Figure 6, for a fixed β value, particularly at the lower β spectrum.

The HTES mass is plotted in Figure 6 as functions of the prime pressure and β. More energy is allocated towards thermal storage with increasing β. Therefore, in general, the HTES mass increases with β in order to achieve the specified and constant HTES temperature swing in each cycle, as shown in Figure 6. For a fixed value of β, at the higher end of its spectrum, the HTES mass given in Figure 6 reaches a minimum as a function of the prime pressure. The prime pressure leading to a minimum HTES mass coincides with that of maximum efficiency, in Figure 2. As the prime pressure increases, the HTES mass also increases due to the decrease in system efficiency; therefore, more energy must be stored as higher turbine mass flow rates are employed to obtain the constant output energy during each cycle. Inversely, at the lower end of the β spectrum, the efficiency of the system increases with prime pressure, therefore the total discharge flow rate and the total necessary HTES mass decrease with increasing prime pressure.

4.3 Capital Cost

The total cost of the storage system per unit of delivered energy, equation (27), is shown in Figure 7. The roundtrip efficiency and air storage price have a dominant influence on the system capital cost, as the air storage price per unit volume is much higher than the HTES cost per unit mass, and the efficiency dictates the necessary storage sizes. Therefore, in general, the cost increases with decreasing efficiency and increasing storage volume. At β=100%, where the air storage volume is identically zero, the cost is purely that of the HTES and its corresponding machinery cost per kilowatt-hour. As the system efficiency decreases, with increasing prime pressure at β=100%, the necessary HTES mass and flow rates, Figure 5 & 6, increase drastically resulting in higher cost. As β decreases, the air storage price begins to influence the system cost as its necessary volume increases. At β values very near 100%, a tank is more cost effective than a cavern, however caverns become more cost effective very quickly as β is decreased from 100%.

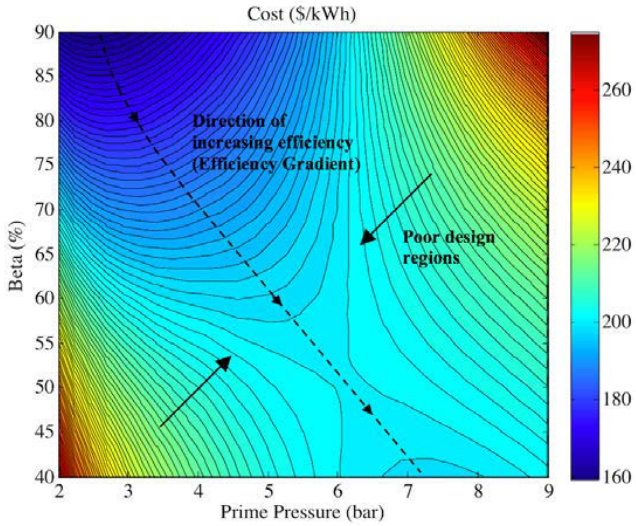

Figure 7: HT-CAES cost ($/kWh), equation (27), as a function of the energy distribution, β, and the prime pressure. The dotted line represents the direction of increasing efficiency (given in Figure 2), which begins at the optimum prime pressure of a regenerative Brayton cycle (at $\boldsymbol{\beta = 100\%}$).

Revisiting the efficiency gradient in Figure 2, and overlapping the efficiency gradient on the cost map results in the dotted line, labeled "Efficiency gradient", in Figure 7. As was demonstrated by Figure 2, any perpendicular deviation from this efficiency gradient results in a lower efficiency than otherwise achievable. Additionally, however, the cost map given by Figure 6 demonstrates that perpendicular deviations from this efficiency gradient also result in a higher cost. Therefore, the efficiency gradient provides a local optimum design region resulting in maximum efficiency and minimum cost. Any deviation perpendicular to the efficiency gradient line results in a higher cost and lower efficiency than otherwise achievable, therefore areas away from this line can be regarded as poor design regions that should be avoided.

In general, the cost of the hybrid storage system increases along the efficiency gradient, or along the local optimum line of operation. In other words, as the reliance on thermal energy storage is increased the cost of the system is decreased, as the system cost becomes leveraged by the cheap thermal energy storage cost. The addition of the turbocharger provides a means of heavily relying on thermal storage, as its additional mass flow rate reduces the reliance on the air storage. Therefore, there exists an inherent trade-off in the hybrid storage cost and efficiency as a function of the energy distribution. The desired point of operation along the efficiency gradient, or the local optimum line of operation, depends on the specific energy application, which the hybrid storage system must integrate with. Energy application priorities are not unique; these priorities may include cost, efficiency and footprint. The efficiency gradient line provides a means of adjusting the system characteristics to meet various application priorities without a change in system capacity. However, tradeoffs between efficiency, cost, and footprint are inherent in the system and quantified through the efficiency, size, and cost maps provided by Figures 2, 6, and 7. A lower system cost and footprint results in a lower efficiency, corresponding to higher thermal energy storage allocation (large β values). On the contrary, higher system efficiency requires a higher capital cost and a larger footprint, corresponding to higher compressed air energy storage allocation (lower β values).

It is imperative to note the existence of a local minimum and maximum in cost along the efficiency gradient, at the lower end of the β spectrum, given by Figure 7. This is caused by the local minimum in storage volume, shown in Figure 6, as a function of the prime pressure at lower β values. The slopes in the vicinity of the local minimum and maximum in cost are quite gradual. Additionally, any further increase in efficiency at β=40%, at the lower end of the efficiency gradient in Figure 7, would require an increase in the prime pressure which would further increase the cost of the system. Therefore, the optimal global maximum and minimum in cost and efficiency reside at the ends of the local optimum line of operation.

4.4 Sensitivity Analysis & Off-Design Performance

This section provides an assessment of the off-design performance pertaining the HT-CAES system. In particular, the sensitivity of the HT-CAES roundtrip efficiency on the various design parameters, presented in Table. 1, is reported and compared with a baseline, defined by the parameter values in Table. 1. The off-design performance and sensitivity analysis is performed on two points (β=50%, and β=90%) along the HT-CAES local optimum line of operation, illustrated in Figures. 2 and 7. These two points are of particular interest as they represent two extremes of the HT-CAES operational spectrum, where β=90% and β=50% characterize a higher TES and CAES dependence, respectively. The percent change in the HT-CAES roundtrip efficiency from the baseline (where the baseline efficiency is given by Figure. 2 at the respective β value, along the optimum operation line) as a function of the percent change in the various parameters from the baseline, given by Table. 1, is shown in Figure. 8. As shown by Figure. 8, the parameters under investigation include the maximum storage pressure, the HTES temperature (or turbine inlet temperature), the compressor and turbine isentropic efficiencies, and the ambient temperature.

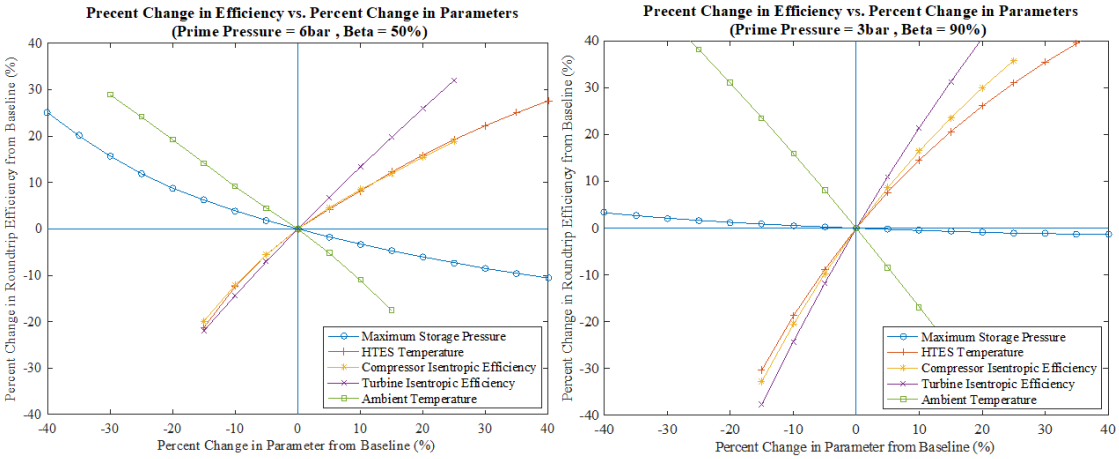

Figure. 8: Percent change in efficiency from baseline (given by the corresponding optimal operation in Figure. 2) vs. percent change in parameters from baseline (given by Table. 1) at two different β values along the optimum line of operation presented in Figure. 2 and Figure. 7.

As depicted by Figure. 8, each plot represents the two β values under investigation, and the same general efficiency sensitivity trends are exhibited in both plots by each parameter. However, the degree of efficiency sensitivity (slope) from each parameter differ quite substantially between both β values. The roundtrip efficiency of the HT-CAES system generally increases with the HTES temperature and isentropic turbine and compressor efficiencies. However, the system efficiency decreases with ambient temperature. As a consequence, the HT-CAES system inherently performs better in winter conditions. Additionally, the roundtrip efficiency of the system decreases with increasing maximum storage pressure. The degree of sensitivity on the efficiency by each parameter is largely dependent on the β value of operation. At higher β values, where the system is more dependent on thermal storage, the efficiency is more sensitive to HTES temperature changes as compared with that of lower β values. Conversely, at lower β values, where the system is more dependent on compressed air storage, the efficiency is more sensitive to maximum storage pressure changes as compared with that of higher β values. In the extreme case of β=100% and the system results in a pure Brayton cycle, the efficiency becomes insensitive to maximum storage pressure changes.

As illustrated in Figure. 8 at β=50%, the efficiency decreases with increasing maximum storage pressure, which is primarily due to the turbocharger. The optimal operation of a stand-alone turbocharger, essentially a Brayton cycle, is depicted by Figure. 2 at β=100%, illustrating a relatively low optimum operating pressure value of 2.53bar. Moreover, As the maximum storage pressure in the system is increased, the prime pressure (or operating pressure) must also increase in order to minimize throttling losses, however this removes the turbocharger function from its optimal operation. Therefore, the HT-CAES system is best designed to operate at lower maximum storage pressures, thereby allowing the turbocharger to operate at its near-optimal conditions. In other words, the turbocharger is utilized most efficiently at a lower maximum storage pressure.

5. Discussion

In this section, a comparison between the HT-CAES system and other energy storage methods is provided and discussed from both a performance and cost perspective. Conventional CAES systems have been studied extensively in the literature and a summary of their reported performance and cost ranges are provided in Table. 2. The upper and lower conventional CAES performance ranges correspond to the cases with and without waste heat utilization respectively. The analysis performed for an AA-CAES is similar to previous works [38], where a comparable configuration given by Figure. 1 is utilized, however the cycle excludes the turbocharger and HTES, and includes a two-stage compressor with inter and after cooling. The same cost methodology applied to the HT-CAES system is also implemented on the AA-CAES system, and the analysis assumes the same output power and isentropic efficiencies provided in Table. 1.

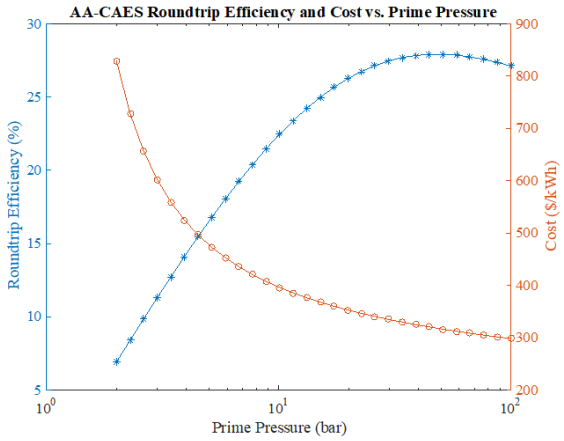

Figure 9: Efficiency and cost of an AA-CAES system as a function of the prime pressure.

Since an AA design stores all energy in the form of compressed air, the variable β=0% by definition and the system is investigated as a function of the prime pressure only. The AA-CAES system cost and efficiency curves are given in Figure. 9b, and illustrate an optimum prime pressure leading to a maximum efficiency of 27.9% and a corresponding cost of 316.3$/kWh. The AA-CAES results assume a heat capacity rate ratio (heat capacity rate of air over that of the heat carrier fluid) of 5. A minimum heat capacity rate ratio of unity results in the highest possible efficiency, 47%, however impractical due to the excessively high compressor exhaust temperatures [38]. A summary of the results associated with the conventional, AA, and HT-CAES system is provided in Table. 2.

Table 2: A summary of the costs and efficiencies corresponding to the various CAES systems

CAES System	Roundtrip Efficiency (%)	Cost ($/kWh)
Conventional CAES [53]	42 - 55	249 - 330
AA-CAES	27.9 - 47	316.3
HT-CAES	24.5 – 57.5	65 - 200

Although the performance of a HT-CAES is comparable to that of a conventional system, the HT-CAES system eliminates combustion emissions, drastically reduces storage and operating pressures, provides additional storage volume/footprint flexibility, and is substantially lower in cost as it operates on lower pressures, which mitigates the need for multi stage compression and expansion. Lastly, the HT-CAES system offers an additional degree of cost freedom, which permits the system to reach costs as low as 65$/kWh. Additionally, as demonstrated by Figure 8, the HT-CAES system performance can be further improved with increasing storage temperature, and decreasing storage pressure.

The capital costs of various other energy storage systems are widely available in the literature. Table. 3 provides a summary of the minimum, average, and maximum reported capital cost values of various available energy storage technologies, along with the calculated HT-CAES system cost for comparison.

Table 3: Reported capital costs of various energy storage systems, from the literature [53], and calculated HT-CAES Cost

Energy Storage Technology	Capital cost, per unit of storage capacity ($/kWh)		
	Minimum	Average	Maximum
CAES	249	312	330
Flywheel	2,201	5,701	29,808
Li-ion battery	546	649	666
Supercapacitors	822	910	1,018
Hydrogen	474	642	927
HT-CAES	65	-	200

The minimum hybrid thermal-compressed air energy storage (HT-CAES) system capital cost, in Table 2 and 3, corresponds to β=100%, which results in pure thermal storage. The maximum HT-CAES capital cost value corresponds to β=40%, where the turbocharger is essentially turned off and the system resembles that of a conventional CAES design with the combustor replaced by the HTES. Moreover, the performance of a conventional CAES system is similar to that of an HT-CAES system at β=40%, assuming a similar storage pressure and turbine inlet temperature. As evident through Table 3, the HT-CAES system is reasonably competitive from a capital cost perspective, as the HT-CAES system cost is leveraged by the cheap thermal storage. The cost of an advanced adiabatic CAES system is typically higher than that of a conventional system due to its need for multistage compression and expansion [38]. Additionally, the performance of an AA-CAES is typically lower in efficiency than that of hybrid system, assuming throttling losses exist, due to its strong dependence on the temperatures captured by the generated heat of compression. In the presence of throttling losses and internal irreversibilities, realistic AA-CAES efficiencies range from 27.9%-47% depending on the temperature limit provided by the generated and stored heat of compression [38]. Therefore, the HT-CAES system provides a competitive design compared to conventional CAES systems and its advanced adiabatic derivative. Moreover, HT-CAES provides a means of adjusting to various footprint and cost requirements, without compromising the storage capacity. It is important to note that further performance improvements, in the HT-CAES system, are possible. As noted in the capital cost section 4.3, the HT-CAES system cost is dominated by the air storage price. Therefore, incorporating intercooling and reheating components can reduce the necessary compression power and increase the potential for regeneration. Thereby improving the performance of the HT-CAES system without a substantial increase in its capital cost per unit of storage capacity.

Although batteries, flywheels, and supercapacitors generally have higher energy efficiencies, their costs are substantially higher than CAES systems. In addition, their lifetime, energy capacity and discharge times are typically lower than CAES systems. These parameters, among others, play a key role in determining the suitable applications that an energy storage technology may provide within the electrical grid. With their unique strengths and weaknesses, it is unlikely that a sole energy storage technology will provide a universal solution. On the contrary, each available energy storage technology may provide an exclusive solution to a specific grid/renewable-integration application. A good metric for comparing various forms of energy storage is the levelized cost of electricity (LCOE), as it considers the energy efficiency, lifetime, capital cost, and maintenance cost of the system. Therefore, in future work, further insight can be gained by comparing the HT-CAES system with various other forms of energy storage from an LCOE perspective.

6. Conclusion

A novel hybrid thermal and compressed air energy storage configuration is developed which has the potential of eliminating combustion emissions and drastically reducing the storage pressure, volume, and cost as compared with conventional CAES and its derivatives. The addition of both thermal energy storage and a turbocharger have the effect of significantly leveraging the cost of the system, as supplementary mass flow rate is provided alongside the stored air, and the cost of thermal storage is considerably cheaper than air storage. The reduced system cost, however, comes at the expense of a reduced efficiency, as the performance of heat engines are bound by the Carnot limit and compressed air energy storage, theoretically, has no such constraint. The hybrid system provides the flexibility of adjusting to a myriad of storage volumes based on available geological restrictions. In addition, the hybrid storage system performs best at low storage pressures, which reduces the complexity as it alleviates the need

for multistage compression and expansion. The thermodynamic optimization results provide the operational efficiency, cost and storage sizing (thermal and air volume) maps, which can be used as a reference in future development endeavors. In addition, all mass flow rate maps are provided, which dictate the necessary machinery sizes. The operational flexibility of HT-CAES is particularly useful as the priorities of various energy applications are not unique, these priorities may include cost, efficiency, and footprint. The hybrid CAES system possesses a wide range of possible operations, without a compromise in its storage capacity, which may prove useful as we move towards a sustainable future.

Nomenclature

HT-CAES	Hybrid Thermal Compressed Air Energy Storage	LTES	Low Temperature Thermal Energy Storage
HTES	High Temperature Thermal Energy Storage	HTF	LTES Heat Transfer Fluid
r_e	Expansion Pressure Ratio	r_c	Compression Pressure Ratio
β	Energy Distribution (equation 1)	η	Component Efficiency
W	Energy of Compression or Expansion	ε	Heat Exchanger Effectiveness
$\dot{W}$	Power of Compression or Expansion	k	Ratio of Specific Heat of Air
Q	Heat Energy	V	Volume
$\dot{Q}$	Heat Power	R	Ideal Gas Constant of Air
P	Pressure	E	Energy
T	Temperature	e	Specific Energy
ρ	Density	h	Specific Enthalpy
M	Mass	u	Specific Internal Energy
$\dot{m}$	Mass Flow Rate	Ξ	Component Cost Function
t	Time of Charge or Discharge	c_p	Specific Heat of Air at Constant Pressure
c_v	Specific Heat of Air at Constant Volume	c_{HTES}	Specific Heat of the HTES
c_{LTES}	Specific Heat of the LTES HTF	t	Charge or Discharge Time
η_I	Roundtrip Energy Efficiency (1st Law Efficiency)	η_{II}	Roundtrip Exergy Efficiency (2nd Law Efficiency)

Acknowledgements
This research was supported by the California Energy Commission, Award no. EPC-14-027.

References

[1] Sun Can, Zhaohong Bie, Zijun Zhang, A new framework for the wind power curtailment and absorption evaluation, International Transactions on Electrical Energy Systems, 2016:2016 vol: 26 iss: 10 pg: 2134 -2147 doi: 10.1002/etep.2194
[2] Li CB, Shi HQ, Cao YJ, et al. Comprehensive review of renewable energy curtailment and avoidance: a specific example in China. Renewable & Sustainable Energy Reviews 2015; 41:1067–1079.
[3] Zou, J (Zou, Jin) ; Rahman, S (Rahman, Saifur) ; Lai, X (Lai, Xu), Mitigation of Wind Output Curtailment by Coordinating with Pumped Storage and Increasing Transmission Capacity, 2015 IEEE POWER & ENERGY SOCIETY GENERAL MEETING
[4] Waite, Modi, V, Modeling wind power curtailment with increased capacity in a regional electricity grid supplying a dense urban demand, 2016, APPLIED ENERGY, Volume: 183 Pages: 299-317 DOI: 10.1016/j.apenergy.2016.08.078
[5] Wang, CX, Study of Unit Commitment Strategies in Combating Wind Curtailment in China, 2015 4TH INTERNATIONAL CONFERENCE ON ENERGY AND ENVIRONMENTAL PROTECTION (ICEEP 2015) Pages: 1137-1140
[6] Fan, Wang, WQ, Shi, RJ, Li, FT, Analysis and countermeasures of wind power curtailment in China, 2015, ENEWABLE & SUSTAINABLE ENERGY REVIEWS, Volume: 52. Pages: 1429-1436, DOI: 10.1016/j.rser.2015.08.025
[7] Gunter, N, Marinopoulos, A , Energy storage for grid services and applications: Classification, market review, metrics, and methodology for evaluation of deployment cases, 2016, JOURNAL OF ENERGY STORAGE, Volume: 8, Pages: 226-234, DOI: 10.1016/j.est.2016.08.011
[8] James E. Mason, Cristina L. Archer, Baseload electricity from wind via compressed air energy storage (CAES), Renewable and Sustainable Energy Reviews, Volume 16, Issue 2, 2012, Pages 1099-1109, ISSN 1364-0321, https://doi.org/10.1016/j.rser.2011.11.009.
[9] Zidar, Matija. Georgilakis, Hatziargyriou, ND, Capuder, T, Skrlec, D, Review of energy storage allocation in power distribution networks: applications, methods and future research, 2016, IET GENERATION TRANSMISSION & DISTRIBUTION, Volume: 10, Issue: 3, Pages: 645-652, Special Issue: SI, DOI: 10.1049/iet-gtd.2015.0447
[10] A.G. Olabi, Renewable energy and energy storage systems, In Energy, Volume 136, 2017, Pages 1-6, ISSN 0360-5442, https://doi.org/10.1016/j.energy.2017.07.054.
[11] Anuta, OH (Anuta, Oghenetejiri Harold)[1] ; Taylor, P (Taylor, Phil)[1] ; Jones, D (Jones, Darren)[2] ; McEntee, T (McEntee, Tony)[2] ; Wade, N(Wade, Neal)[1], An international review of the implications of regulatory and electricity market structures on the emergence of grid scale electricity storage, 2014, RENEWABLE & SUSTAINABLE ENERGY REVIEWS, Volume: 38, Pages: 489-508, DOI: 10.1016/j.rser.2014.06.006
[12] Hameer, S , van Niekerk, JL , A review of large-scale electrical energy storage, 2015, INTERNATIONAL JOURNAL OF ENERGY RESEARCH, Volume: 39, Issue: 9, Pages: 1179-1195, DOI: 10.1002/er.3294
[13] Freeman, E , Occello, D , Barnes, F , Energy storage for electrical systems in the USA, 2016, AIMS ENERGY, Volume: 4, Issue: 6, Pages: 856-875, DOI: 10.3934/energy.2016.6.856

[14] S. Karellas, N. Tzouganatos, Comparison of the performance of compressed-air and hydrogen energy storage systems: Karpathos island case study, Renewable and Sustainable Energy Reviews, Volume 29, 2014, Pages 865-882, ISSN 1364-0321, https://doi.org/10.1016/j.rser.2013.07.019.
[15] Obi, M, Jensen, SM , Ferris, JB, Bass, RB , Calculation of levelized costs of electricity for various electrical energy storage systems, 2017, RENEWABLE & SUSTAINABLE ENERGY REVIEWS, Volume: 67, Pages: 908-920, DOI: 10.1016/j.rser.2016.09.043
[16] Erren Yao, Huanran Wang, Ligang Wang, Guang Xi, François Maréchal, Multi-objective optimization and exergoeconomic analysis of a combined cooling, heating and power based compressed air energy storage system, Energy Conversion and Management, Volume 138, 15 April 2017, Pages 199-209, ISSN 0196-8904, http://dx.doi.org/10.1016/j.enconman.2017.01.071.
[17] Wei Ji, Yuan Zhou, Yu Sun, Wu Zhang, Baolin An, Junjie Wang, Thermodynamic analysis of a novel hybrid wind-solar-compressed air energy storage system, Energy Conversion and Management, Volume 142, 15 June 2017, Pages 176-187, ISSN 0196-8904, http://dx.doi.org/10.1016/j.enconman.2017.02.053.
[18] Adriano Sciacovelli, Yongliang Li, Haisheng Chen, Yuting Wu, Jihong Wang, Seamus Garvey, Yulong Ding, Dynamic simulation of Adiabatic Compressed Air Energy Storage (A-CAES) plant with integrated thermal storage – Link between components performance and plant performance, Applied Energy, Volume 185, Part 1, 1 January 2017, Pages 16-28, ISSN 0306-2619, http://dx.doi.org/10.1016/j.apenergy.2016.10.058.
[19] Daniel Wolf, Marcus Budt, LTA-CAES – A low-temperature approach to Adiabatic Compressed Air Energy Storage, Applied Energy, Volume 125, 15 July 2014, Pages 158-164, ISSN 0306-2619, http://dx.doi.org/10.1016/j.apenergy.2014.03.013.
[20] Hao Peng, Yu Yang, Rui Li, Xiang Ling, Thermodynamic analysis of an improved adiabatic compressed air energy storage system, Applied Energy, Volume 183, 1 December 2016, Pages 1361-1373, ISSN 0306-2619, http://dx.doi.org/10.1016/j.apenergy.2016.09.102.
[21] Adewale Odukomaiya, Ahmad Abu-Heiba, Kyle R. Gluesenkamp, Omar Abdelaziz, Roderick K. Jackson, Claus Daniel, Samuel Graham, Ayyoub M. Momen, Thermal analysis of near-isothermal compressed gas energy storage system, Applied Energy, Volume 179, 1 October 2016, Pages 948-960, ISSN 0306-2619, http://dx.doi.org/10.1016/j.apenergy.2016.07.059.
[22] Gayathri Venkataramani, Prasanna Parankusam, Velraj Ramalingam, Jihong Wang, A review on compressed air energy storage – A pathway for smart grid and polygeneration, Renewable and Sustainable Energy Reviews, Volume 62, September 2016, Pages 895-907, ISSN 1364-0321, http://dx.doi.org/10.1016/j.rser.2016.05.002.
[23] Seamus D. Garvey and Andrew Pimm, Chapter 5 - Compressed Air Energy Storage, In Storing Energy, edited by Trevor M. Letcher, Elsevier, Oxford, 2016, Pages 87-111, ISBN 9780128034408, http://dx.doi.org/10.1016/B978-0-12-803440-8.00005-1.
[24] Odukomaiya, A ,Abu-Heiba, A ,Gluesenkamp, KR , Abdelaziz, O,Jackson, RK , Daniel, C ,Graham, S ,Momen, AM , Thermal analysis of near-isothermal compressed gas energy storage system, 2016, APPLIED ENERGY, Volume: 179, Pages: 948-960, DOI: 10.1016/j.apenergy.2016.07.059
[25] Kilic, M , Mutlu, M , A novel design of a compressed air storage system with liquid pistons, 2016, BULGARIAN CHEMICAL COMMUNICATIONS, Volume: 48, Pages: 318-324, Special Issue: E2
[26] Li, PY , Saadat, M , An approach to reduce the flow requirement for a liquid piston near-isothermal aircompressor/expander in a compressed air energy storage system, 2016, IET RENEWABLE POWER GENERATION, Volume: 10, Issue: 10, Pages: 1506-1514, Special Issue: SI, DOI: 10.1049/iet-rpg.2016.0055
[27] Qin, C, Loth, E , Liquid piston compression efficiency with droplet heat transfer, 2014, APPLIED ENERGY, Volume: 114, Pages: 539-550, Special Issue: SI, DOI: 10.1016/j.apenergy.2013.10.005
[28] Daniel Buhagiar, Tonio Sant, Modelling of a novel hydro-pneumatic accumulator for large-scale offshore energy storage applications, In Journal of Energy Storage, 2017, ISSN 2352-152X, https://doi.org/10.1016/j.est.2017.05.005.
[29] Marcus Budt, Daniel Wolf, Roland Span, Jinyue Yan, A review on compressed air energy storage: Basic principles, past milestones and recent developments, In Applied Energy, Volume 170, 2016, Pages 250-268, ISSN 0306-2619, https://doi.org/10.1016/j.apenergy.2016.02.108.
[30] Qin, C , Loth, E ,Simulation of spray direct injection for compressed air energy storage, 2016, APPLIED THERMAL ENGINEERING, Volume: 95, Pages: 24-34. DOI: 10.1016/j.applthermaleng.2015.11.008
[31] McBride T, Bell A, Kepshire D. ICAES innovation: foam-based heat exchange. USA: Seabrook; 2013.
[32] Kentschke T. Druckluftmaschinen als Generatorantrieb inWarmluftspeichern. Dissertation. Clausthal; 2004.
[33] Lukasz Szablowski, Piotr Krawczyk, Krzysztof Badyda, Sotirios Karellas, Emmanuel Kakaras, Wojciech Bujalski, Energy and exergy analysis of adiabatic compressed air energy storage system, In Energy, Volume 138, 2017, Pages 12-18, ISSN 0360-5442, https://doi.org/10.1016/j.energy.2017.07.055.
[34] Hao Peng, Yu Yang, Rui Li, Xiang Ling, Thermodynamic analysis of an improved adiabatic compressed air energy storage system, In Applied Energy, Volume 183, 2016, Pages 1361-1373, ISSN 0306-2619, https://doi.org/10.1016/j.apenergy.2016.09.102.
[35] Baghaei Lakeh R., Villanava, I., Houssainy, S., Anderson, K., Kavehpour, H.P., 2016, Design of a Modular Solid-Based Thermal Energy Storage for a Hybrid Compressed Air Energy Storage System, Paper No. PowerEnergy2016-59160, Proc. of 2016 ASME Int. Conference on Energy Sustainability Charlotte, NC
[36] Houssainy, S Baghaei Lakeh R., Kavehpour, H.P., 2016, A Thermodynamic Model of High Temperature Hybrid Compressed Air Energy Storage System for Grid Storage, Paper No. PowerEnergy2016-59431, Proc. of 2016 ASME Int. Conference on Energy Sustainability Charlotte, NC
[37] Ip PP, Houssainy S, Kavehpour. Modeling of a Low Cost Thermal Energy Storage System to Enhance Generation From Small Hydropower Systems. 2017, ASME Power Conference, doi:10.1115/POWER-ICOPE2017-3684
[38] Sammy Houssainy, Mohammad Janbozorgi, Peggy Ip, Pirouz Kavehpour, Thermodynamic Analysis of a High Temperature Hybrid Compressed Air Energy Storage (HTH-CAES) System, Renewable Energy, Available online 12 September 2017, ISSN 0960-1481, https://doi.org/10.1016/j.renene.2017.09.038.
[39] Peng, H , Yang, Y , Li, R , Ling, X , Thermodynamic analysis of an improved adiabatic compressed air energy storage system, 2016, APPLIED ENERGY, Volume: 183, Pages: 1361-1373, DOI: 10.1016/j.apenergy.2016.09.102
[40] Wolf D, Budt M. LTA-CAES – a low-temperature approach to adiabatic compressed air energy storage. Appl Energy 2014;125:158–64.
[41] Luo, X ,Wang, JH, Krupke, C, Wang, Y , Sheng, Y ,Li, J ,Xu, YJ, Wang, D, Miao, SH , Chen, HS , Modelling study, efficiency analysis and optimisation of large-scale Adiabatic Compressed Air Energy Storage systems with low-temperature thermal storage, 2016, APPLIED ENERGY, Volume: 162, Pages: 589-600, DOI: 10.1016/j.apenergy.2015.10.091

[42] B. Cárdenas, A.J. Pimm, B. Kantharaj, M.C. Simpson, J.A. Garvey, S.D. Garvey, Lowering the cost of large-scale energy storage: High temperature adiabatic compressed air energy storage, In Propulsion and Power Research, Volume 6, Issue 2, 2017, Pages 126-133, ISSN 2212-540X, https://doi.org/10.1016/j.jppr.2017.06.001.
[43] V. de Biasi, Fundamental analyses to optimize adiabatic CAES plant effi- ciencies, Gas Turbine World 39 (2009) 26e28.
[44] Doetsch C, Budt M, Wolf D, Kanngießer A. Adiabates Niedertemperatur- Druckluftspeicherkraftwerk zur Unterstützung der Netzintegration von Windenergie. Abschlussbericht zu FKZ 0325211; 2012.
[45] Barbour E, Mignard D, Ding Y, Li Y. Adiabatic compressed air energy storage with packed bed thermal energy storage. Appl Energy 2015;155:804–15.
[46] Dreißigacker V, Zunft S, Müller-Steinhagen H. A thermo-mechanical model of packed-bed storage and experimental validation. Appl Energy 2013;111:1120–5.
[47] Yang Z, Wang Z, Ran P, Li Z, Ni W. Thermodynamic analysis of a hybrid thermal-compressed air energy storage system for the integration of wind power. Applied Thermal Engineering 2014;66:519-527.
[48] Ibrahim Dincer, Marc Rosen, Thermal Energy Storage Systems and Applications (2nd Edition), 2011, John Wily & Sons Ltd, United Kingdom
[49] Ibrahim Dincer, Marc Rosen, Pouria Ahmadi, Optimization of Energy Systems, 2017, Wily, ISBN: 978-1-118-89443-9
[50] Hossein Pirouz KAVEHPOUR, Hamarz ARYAFAR, Ariana THACKER, Mohammad JANBOZORGI, Sammy HOUSSAINY, Walid ISMAIL, The Regents of the University of California, Low-Cost Hybrid Energy Storage System, United States Patent, WO2017044658 A1, 2017 March 16.
[51] Agazzani AA, Massardo AF. A Tool for Thermoeconomic Analysis and Optimization of Gas, Steam, and Combined Plants. ASME. Eng. Gas Turbines Power. 1997;119(4):885-892. Doi:10.1115/1.2817069.
[52] Nikhil, Dev, et al. "Economic and performance analysis of thermal system." *Research Journal of Recent Sciences* 1.4 (2012): 57-59.
[53] Zakeri, Behnam & Syri, Sanna. Electrical energy storage systems A comparative life cycle cost analysis Renewable and Sustainable Energy Reviews, 42 (2015) 569-596